World Academy of Science, Engineering and Technology
International Journal of Mechanical and Mechatronics Engineering
Vol:11, No:1, 2017

H-Infinity Controller Design for the Switched Reluctance Machine

Siwar Fadhel, Imen Bahri, Man Zhang

***Abstract*—**The switched reluctance machine (SRM) has undeniable qualities in terms of low cost and mechanical robustness. However, its highly nonlinear character and its uncertain parameters justify the development of complicated controls. In this paper, authors present the design of a robust H-infinity current controller for an 8/6 SRM with taking into account the nonlinearity of the SRM and with rejection of disturbances. The electromagnetic torque is indirectly regulated through the current controller. To show the performances of this control, a robustness analysis is performed by comparing the H-infinity and PI controller simulation results. This comparison demonstrates better performances for the presented controller. The effectiveness and robustness of the presented controller are also demonstrated by experimental tests.

***Keywords*—**Current regulation, experimentation, robust H-infinity control, switched reluctance machine.

I. Introduction

THE SRM presents an interesting candidate for electrical vehicles thanks to its simple structure, mechanical robustness, and low cost. However, SRM has larger torque ripple and noise compared to other types of machines. These disadvantages may be ameliorated either by modifying the motor design [1] or by developing a good control of the motor [2]. The second solution is often used. Generally, for an efficient torque control in electrical machines, the current control which forms the heart of the control must be efficient. Several researches have contributed to the development of linear and nonlinear controls of the SRM. Among these techniques used for the speed control, the feedback-linearization [3], the passivity- based control [4] and sliding mode control [5] are proposed. A current regulator with gain-scheduling PI [6], a hysteresis controller (also called ON-OFF) [7], and a neural and fuzzy logic control [8] are utilized for the current control. These control methods require often an accurate model of the SRM. As being based on an accurate nonlinear model of the machine, the development of these controls is always complicated. On the other hand, as developing an accurate nonlinear model is difficult due to manufacturing tolerances and parameter drift during operation, the developed controller should be robust against model inaccuracies and parameter variations. Yet, this robustness is not considered in the controller design steps and is not always verified. H-infinity is a powerful technique used to design a robust controller for linear systems under uncertainties, parameter variations, and disturbances. This technique can be extended to be applicable for nonlinear systems by means of additional compensations or adaptations. In this paper, the authors propose a robust H-infinity (H_∞) current controller for an 8/6 SRM. The synthesis of this controller uses three filters that are precisely chosen to meet the required specifications (good tracking performance, rejection disturbances and robustness against parameter variations). Performances and stability of the controller are verified by simulations in frequency domain and compared to the ones of PI regulator which demonstrates little advantages for the H-infinity controller. Experimentation has also carried out to demonstrate the effectiveness of the proposed approach. In references [9], [10], the authors propose a H_∞ current controller design for the SRM; however, there is no adaptation used to cope with the nonlinear nature of the SRM. In this work, after generating the controller, its gains are adjusted to be suited for the SRM features and overcome the problem of nonlinearity. This adjustment is based on online value of the incremental inductance. The results demonstrate better performances in terms of stability and disturbances rejection comparing with a classical PI controller. This paper is organized as follows. Section II presents the mathematical model of the 8/6 SRM. Section III describes the design of the proposed control. The performances of this controller are verified with simulations in Section IV and then confirmed by experimentation in Section V. Conclusion and discussions end the paper.

II. Mathematical Model of the SRM

The proposed controller is designed for a four-phased SRM. The design of this controller is based on the electromagnetic characteristics of the machine. The non-linearity of this machine is due to the variation of the phase inductance depending on the phase rotor positions. The mathematical model of the SRM is given by equations below. The voltage applied to the phase is expressed as:

$$u = Ri + \frac{d\phi(i,\theta_e)}{dt} \quad (1)$$

Siwar Fadhel is with Group of Electrical Engineering, Paris (GeePs), CNRS UMR 8507; Centrale Supelec; Univ. of Pierre and Marie Curie P6; Univ. of Paris-Sud; Univ. of Paris Saclay, France, National Engineering School of Sousse, Univ. of Sousse, Tunisia (e-mail: siwar_fadhel@yahoo.fr).

Imen Bahri and Man Zhang are with GeePs. (e-mail: imen.bahri@geeps.centralesupelec.fr, man.zhang@Supelec.fr).

with:

$$\phi = L(i,\theta_e)i \tag{2}$$

$$\frac{d\varphi(i,\theta_e)}{dt} = L(i,\theta_e)\frac{di}{dt} + i\frac{dL(i,\theta_e)}{dt} \tag{3}$$

$$\frac{d\varphi(i,\theta_e)}{dt} = L(i,\theta_e)\frac{di}{dt} + i\left(\frac{dL(i,\theta_e)}{dt}\frac{d\theta_e}{dt} + \frac{dL(i,\theta_e)}{dt}\frac{di}{dt}\right) \tag{4}$$

With u: The voltage applied to the terminals of a phase; R: The resistance of a phase; i: The phase current; φ: The linkage flux in a phase; θ_e: The electrical position of the rotor.

From (1) and (4), the phase voltage can be written as

$$u = Ri + \left(L(i,\theta_e) + i\frac{dL(i,\theta_e)}{dt}\right)\frac{di}{dt} + iw_e\frac{dL(i,\theta_e)}{d\theta_e} \tag{5}$$

We note that:

$$L_{inc}(i,\theta_e) = \frac{d\varphi(i,\theta_e)}{di} = L(i,\theta_e) + i\frac{dL(i,\theta_e)}{di} \tag{6}$$

$$e = iw_e\frac{dL(i,\theta_e)}{d\theta_e} \tag{7}$$

Finally, (1) is written as follows:

$$u = Ri + L_{inc}(i,\theta_e)\frac{di}{dt} + e \tag{8}$$

where w_e is the electrical angular velocity, e is the back E.M.F and $L_{inc}(i,\theta_e)$ is the incremental inductance. Equation (8) shows that the SRM is represented by a nonlinear model. The terms $L_{inc}(i,\theta_e)$ and e are calculated by using the analytical expression of the inductance which varies with the current and rotor position. Equation (8) demonstrates that the back E.M.F is a source of disturbance to compensate in the design of the controller. The SRM incremental inductance profile as a function of electrical position and phase current is given in Fig. 1.

The electromagnetic torque is expressed by (9):

$$T(i,\theta_e) = \frac{1}{2}i^2\frac{dL(i,\theta_e)}{d\theta_e} \tag{9}$$

The 3-D views of the flux-linkage and the electromagnetic torque are given in Figs. 2 and 3.

III. Design of the H-Infinity Controller

A. Standard Form

The block diagram considered for the standard H-infinity synthesis is illustrated in Fig. 4.

The standard H_∞ problem consists in finding an optimal value $\gamma \simeq 1$, and a controller K(s) stabilizing the closed loop shown in Fig. 4, and guaranteeing the following inequality:

$$\left\| \begin{matrix} W_1(s).S(s) & W_1(s).S(s).G(s).W_3(s) \\ W_2(s).K(s).S(s) & W_2(s).T(s).W_3(s) \end{matrix} \right\|_\infty < \gamma \tag{10}$$

where G(s) is the system transfer function, S(s) is the sensitivity function whose expression is $(1+K(s).G(s))^{-1}$, and T(s) = K(s).S(s).G(s).

Using condition (9), we infer:

$$|S(s)| < \frac{\gamma}{|W1(s)|};\ |K(s).S(s)| < \frac{\gamma}{|W2(s)|}\ |S(s).G(s)| < \frac{\gamma}{|W1(s).W3(s)|};\ |T(s)| < \frac{\gamma}{|W2(s).W3(s)|} \tag{11}$$

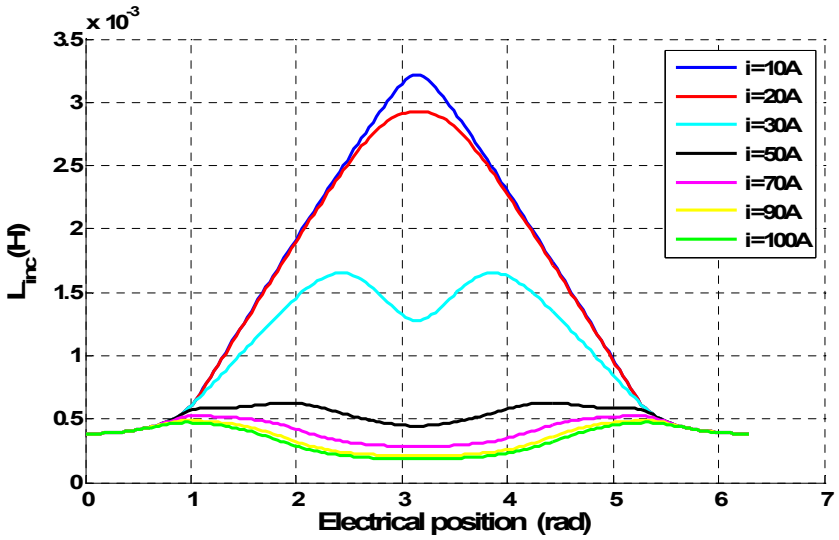

Fig. 1 Incremental inductance for one phase

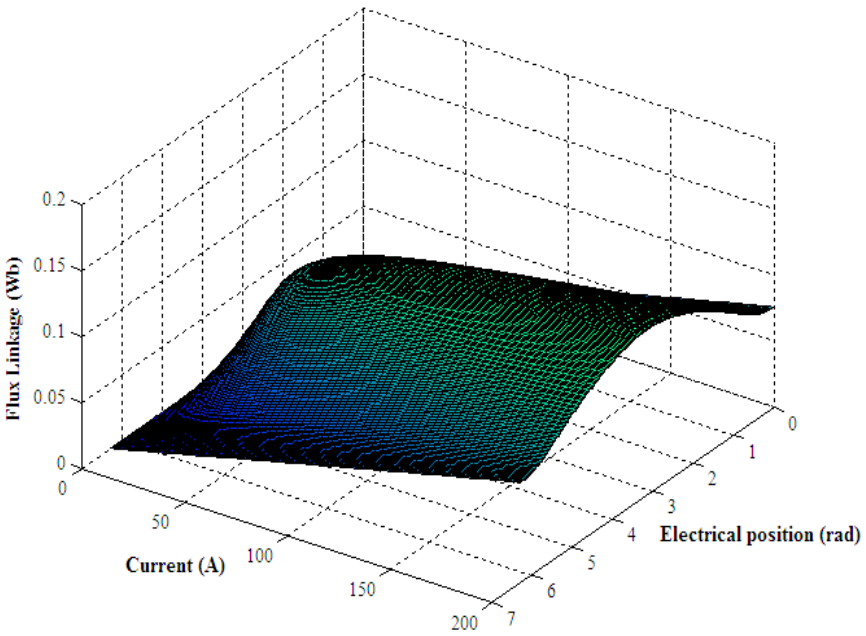

Fig. 2 3-D view of flux-linkage characteristic

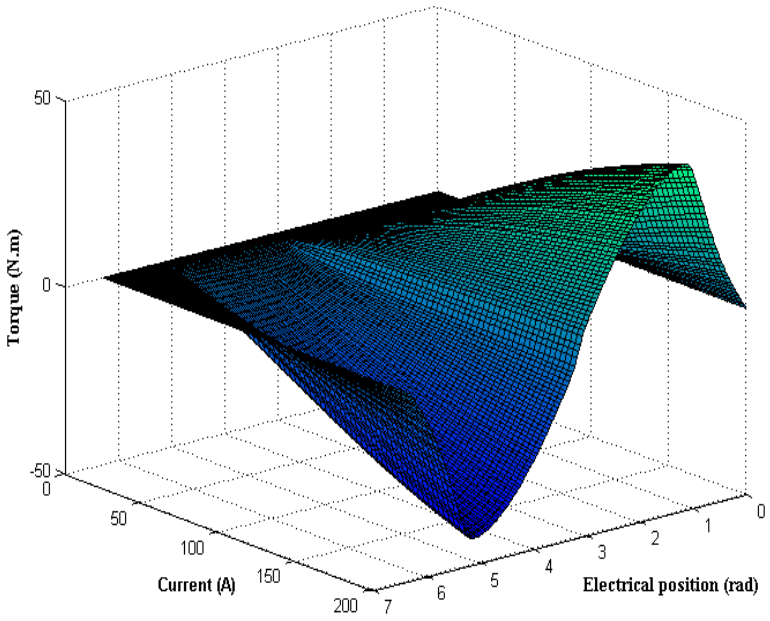

Fig. 3 3-D view of electromagnetic torque characteristic

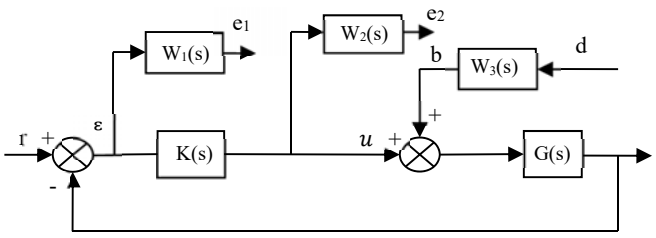

Fig. 4 Closed-loop scheme with the weighting transfer functions

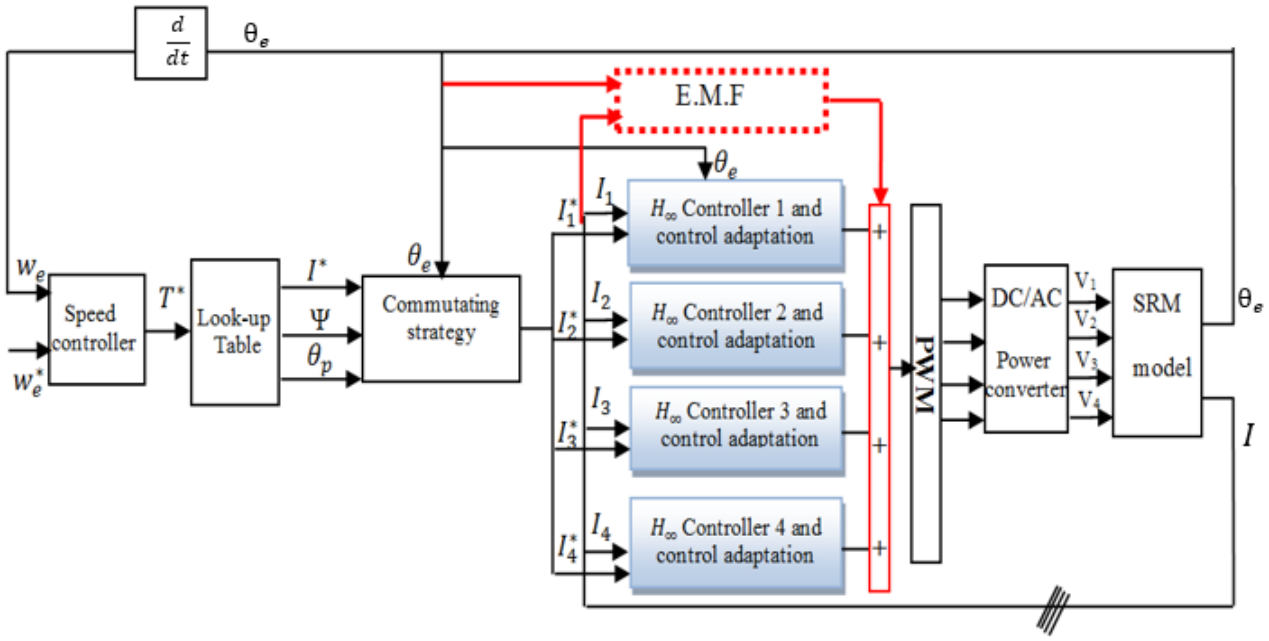

Fig. 5 Overall structure of the SRM control

The desired performances are introduced through the weighting functions $W_1(s)$, $W_2(s)$, and $W_3(s)$ which have the structure of a first-order function (12). These functions are used to generate an optimal controller utilizing the MATLAB function "*hinfsyn*". The H_∞ algorithm is an iterative scheme which allows the designer to refine the first controller obtained from the performances and robustness analysis tools. For this purpose, weighting functions would be readjusted according to the obtained simulation results. In this study, the SRM is modeled as a linear system obtained from (8) and after compensating the effect of the back E.M.F. The nonlinearity caused by the variation of the inductance function of the position and the current is compensated thereafter, as shown in Fig. 6. To develop the controller, the minimum incremental inductance is chosen for this synthesis as an operating point. To consider the variation in the incremental inductance value versus the current and the electrical position of the rotor, we add a stage of compensation to the command obtained at the output of the controller based on the online inductance value. Then, we compensate the back E.M.F to cancel the static error. As a result, the current control loop is as follows:

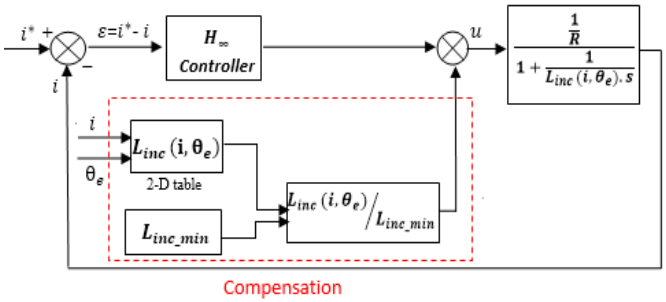

Fig. 6 Block diagram of the current loop

B. Choice of the Weighting Functions and Controller Expression

The weighting functions are given by this expression:

$$W_i = \frac{G_\infty \sqrt{|G_0^2-1|}\ s+G_0 2\pi f_0 \sqrt{|G_\infty^2-1|}}{\sqrt{|G_0^2-1|}\ s+2\pi f_0 \sqrt{|G_\infty^2-1|}} \quad (12)$$

where: G_0, G_∞, and f_0 represent the static gain, the infinity gain, and the cutoff frequency, respectively.

C. Choice of W_1

The choice of $1/W_1$ has been made from the specifications on the tracking performances which are as follows:

- Bandwidth of 2000 rad/s to ensure rapid response time
- Module margin of 0.9
- Low gain at low frequency ($<f_0$), here we fixed 10^{-3} for G_0

The numerical weighting function W_1 is given by:

$$W_1(s) = \frac{0.9s + 871.8}{s + 0.8718} \quad (13)$$

D. Choice of W_2

Here, we specify a cutoff frequency for W_2 to minimize the controller gain at high frequency, in order to reduce the sensitivity to noise that is not considered for these synthesis steps. The other parameters are chosen to keep an optimal value of $\gamma \simeq 1$, and the expression of W_2 is:

$$W_2(s) = \frac{s + 3.145.10^4}{s + 10^5} \quad (14)$$

E. Choice of W_3

The main effect of this filter is to ensure rejection of disturbances, for this purpose it can be chosen as a constant function. For our synthesis, W_3 (s) = 0.9 s ensures a maximum rejection disturbance. The bode diagrams of sensitivity function S, Ks function, SG function, and T function are plotted in Fig. 7, with comparison to the designed weighting functions. This figure shows that the four conditions in (11) are verified.

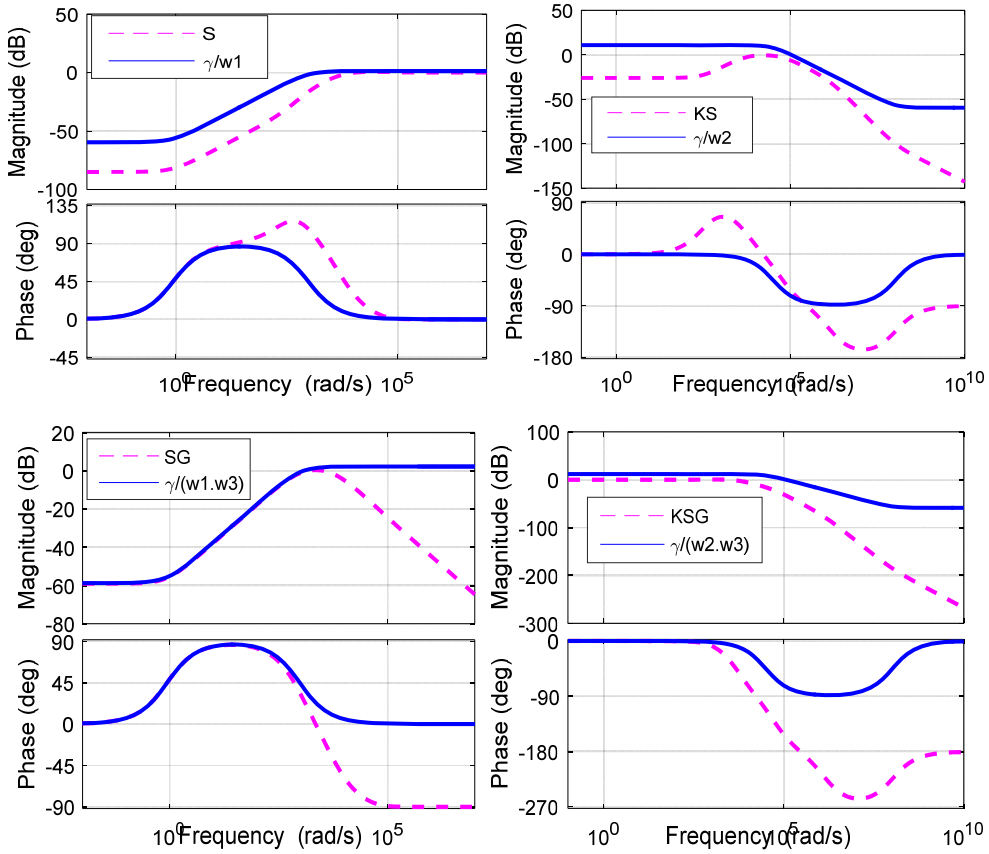

Fig. 7 Frequency responses

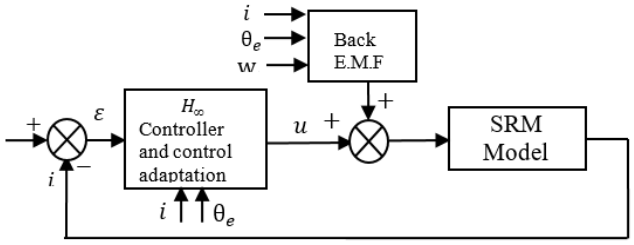

Fig. 8 Current control loop

The resulting controller has the following expression:

$$K(s) = \frac{722.8s^2 + 7.577.10^{10}s + 6.387.10^{13}}{s^3 + 1.407.10^6 s^2 + 8.228.10^{10}s + 7.173.10^{10}} \quad (15)$$

In order to limit its complexity and provide a simple structure especially for practical implementation, this controller is reduced by using the MATLAB function "reduce", which gives a controller as a second-order transfer function giving by:

$$K(s) = \frac{4.99310^4 s + 4.04.10^7}{s^2 + 5.206.10^4 s + 4.538.10^4} \quad (16)$$

The final control loop is shown in Fig. 8.

IV. Simulation Results

The SRM is controlled in speed through an outer loop speed control using a conventional PI and four inner loops for current regulation. The synoptic of the current controller for the SRM is shown in Fig. 5. We note that the average torque control strategy is used in this study. The speed controller provides the total torque reference, which is considered as an average torque over one conducting period. Then, this torque is distributed over the four phases according to the position of the rotor. The control of the average torque is ensured by the adjustment of three control variables, to wit, the current I*, the phase turn-on angle ψ, and the conduction period θ_p. A lot of combinations of these control variables can produce the same average torque at one specific speed. Therefore, they must be optimized for efficiency or low torque ripples criteria. In this study, minimization of the torque ripples is privileged, therefore an

optimal set of these three control variables (ψ, θ_p, I*) over the entire operating range is chosen. After that, they are stored in a look-up table. The linear data interpolation is performed on-line to compute the optimal control parameters depending on the operating point. The simulations are performed by using MATLAB/Simulink for a sampling period Te of 100 µs. The simulation results are shown in Fig. 9 using the designed controller while the motor is operating at 500 rpm. It illustrates the current profile produced by the four phases of the motor, the speed response and the produced torque. From this curve, we can see that the H_∞ current controller achieves the desired performance listed in specifications. As a result of the current regulation, the torque regulation is ensured as well.

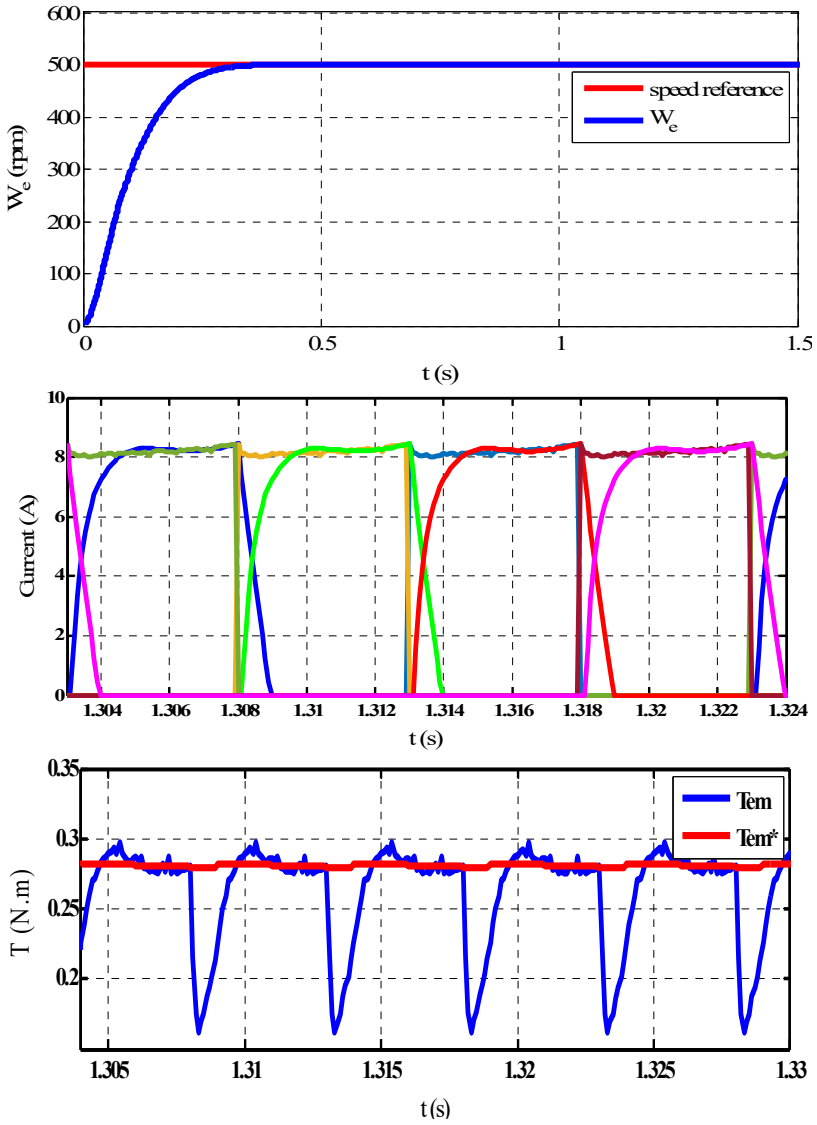

Fig. 9 Simulation results of four phases at a speed equal to 500 rpm, 0Nm

A. Robustness Analysis in Frequency Domain

The dynamic performance of the SRM controller could be affected by the parameters variation. The H_∞ controller's gains are adapted versus the online inductance variation as explained in section III in order to control the dynamic of the system. Table I reports the dynamic variation of the H_∞ controller compared with a conventional PI which is designed with the same bandwidth (2000 rad/s) as the H_∞. The comparison is given for three specific rotor positions (the opposition θ_e=0°, intermediate position θ_e=90°; the conjunction θ_e=180°). Fig. 10 illustrates the bode diagram of the closed current loop simulated for the three positions. This diagram shows that with the gains adaptation of the H_∞ controller, the dynamic does not vary depending on the inductance change, and a large bandwidth is guaranteed. However, in the case of PI controller, when the inductance value increases to its maximum, a 28% of bandwidth loss occurs. We notice that the H_∞ controller guarantees also better stability margin compared to the conventional PI controller and smaller response time as guaranteeing larger bandwidth.

TABLE I
CONTROLLER PERFORMANCES

$\Theta_e(°)$	$L(mH)$	$w_{n,H\infty}(rad/s)$	$w_{n,PI}(rad/s)$	$\Delta\Phi_{BO,H_\infty}(°)$	$\Delta\Phi_{BO,PI}(°)$
0	0.38	1940	1770	72.9	63.7
90	1.8	921	858	44.9	33.5
180	3.22	691	645	34.8	25.4

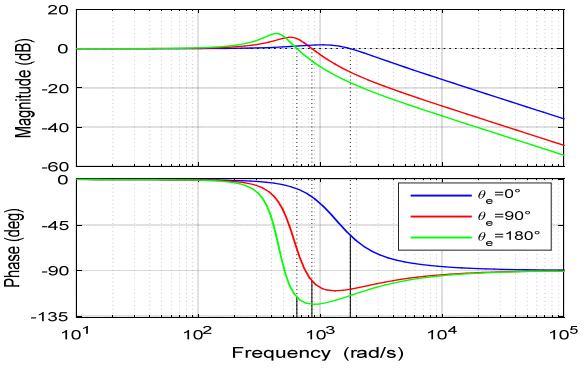

(a)

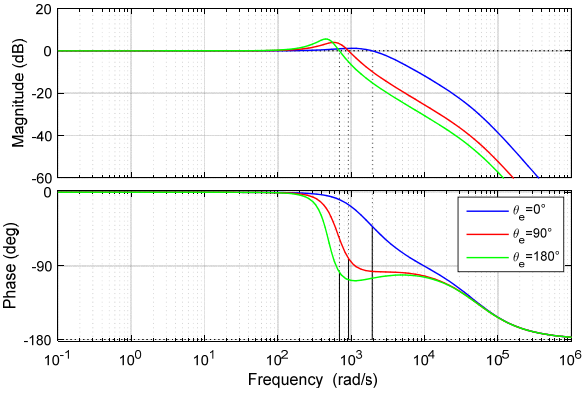

(b)

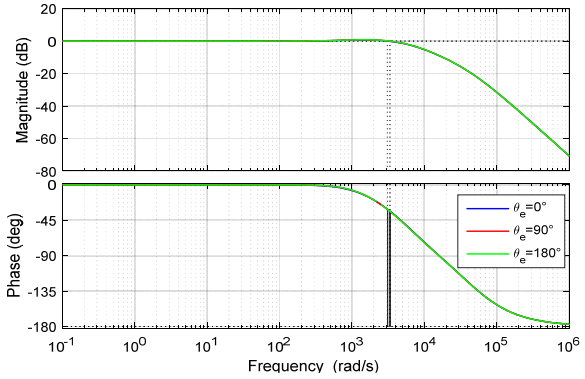

(c)

Fig. 10 Bode diagram of the closed loop current with PI (a), H∞ without adaptation stage (b), H∞ with adaptation stage (c)

B. Robustness Analysis in Time Domain

In this section, the robustness of the proposed current controller against uncertainty and variation of electrical parameters (respectively (L and R)) is considered and simulated with the MATLAB/Simulink SRM model. Afterwards, the robustness against disturbance, such as resistance torque variation, is analyzed. A variation of ±50% and ±20% of the resistance value R and the inductance value L, respectively, is considered at 500 rpm. The current phase curves are represented in Fig. 11. In fact, the variation introduced on the resistance value does not affect the current response and proves that H_∞ current loop is less sensitive to parameters variation. However, the inductance variation introduces a small deviation while keeping a good tracking of the current reference. So, we can note that this control guarantees a good robustness against the uncertainty in parameters.

Fig. 12 shows the speed curve with a 1 N.m load torque introduced at 0.5 s for a speed equal to 500rpm. This curve indicates that the regulator is capable to reject the disturbance.

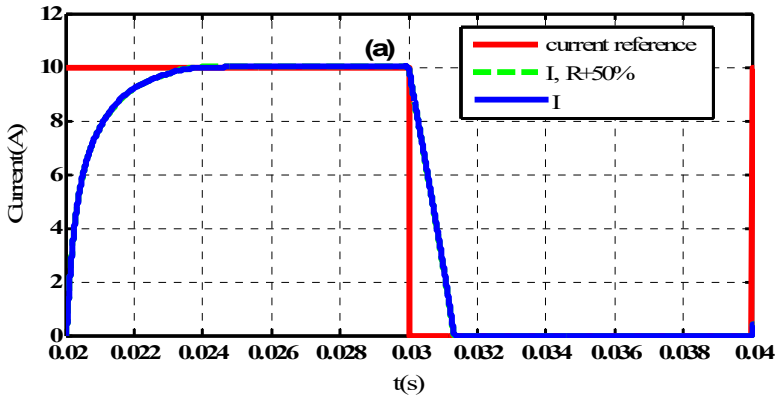

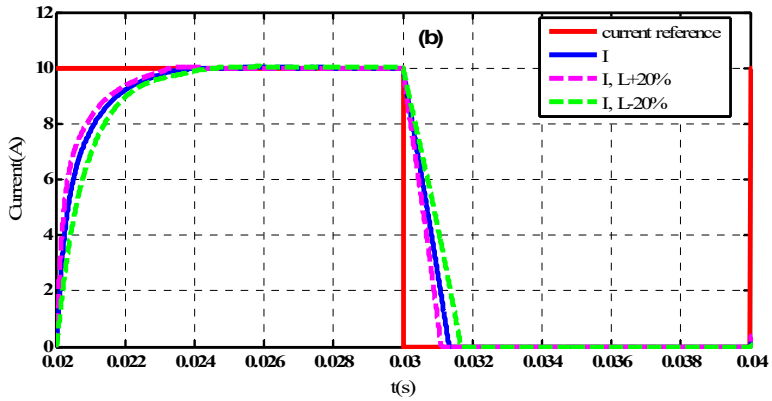

Fig. 11 Robustness test against resistance variation (a), and inductance variation (b)

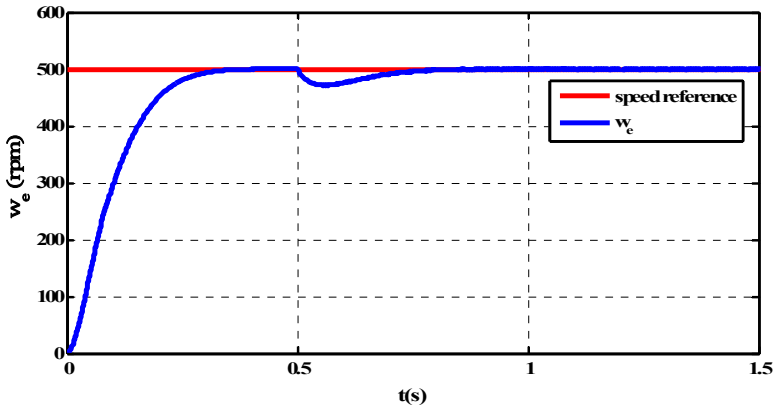

Fig. 12 Disturbance rejection for 1N.mat speed equal to 500 rpm

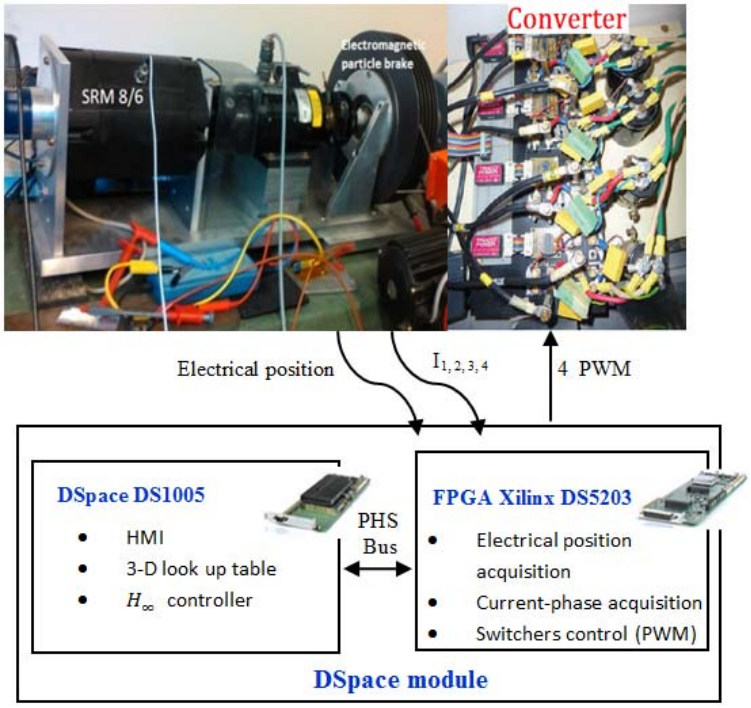

Fig. 13 Experimental test bench

V. Experimental Validation

The experimental validation has been achieved through the test bench illustrated in Fig. 13. This experimental test bench is subdivided in three parts. The first one is a digital control unit which is based on a DSpace platform. It consists of two programmable targets: A Xilinx FPGA card of Virtex5's family and a DSpace DS1005 card for the implementation of the control algorithm. The second one consists of an SRM 8/6, coupled to an electromagnetic particle brake in order to vary the resistance torque, and a four-phased inverter. The third one is the measuring part. It consists of current sensors to measure the four-phased current, and an encoder to measure the rotor angular position, and speed of the SRM. This implementation has been carried out based on a co-design method. The FPGA is used to measure acquisition (rotor position, four-phased current) and to generate the four MLI signals to command the converter. The Human Machine Interface (HMI), the 3-D table that gives the optimal parameters and the H_∞ controller have been implemented in the DSP card. The controller is discretized with a step of 200 µs. The experimental results shown in Fig. 14 illustrate the current profile for one phase at a speed equal to 500 rpm with an electromagnetic torque of 3 N.m, and Fig. 15 presents the speed waveform which shows the disturbance rejection under varying the torque.

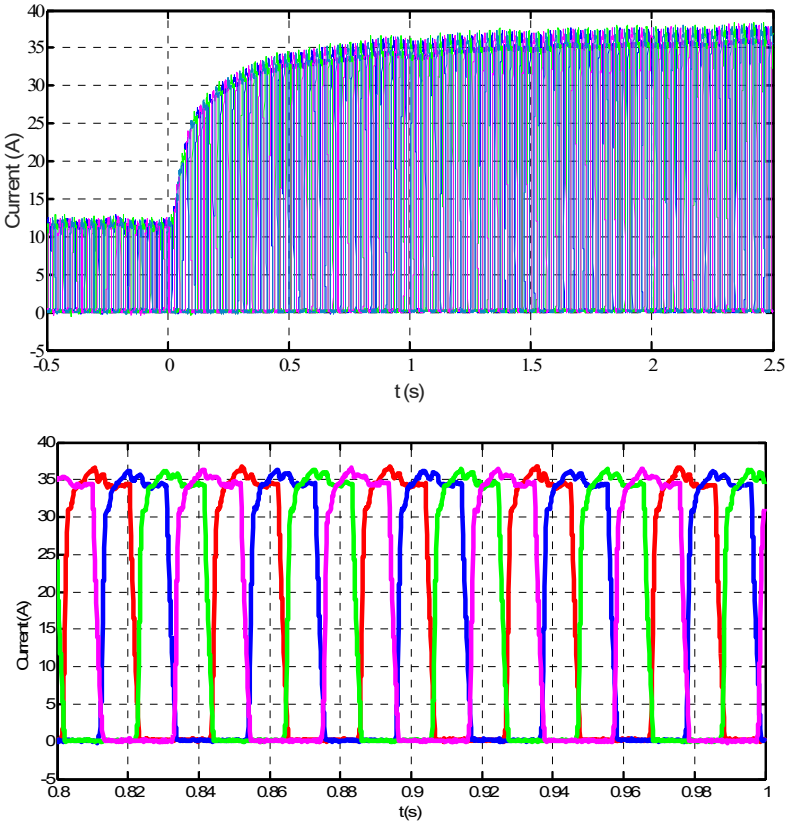

Fig. 14 Experimental results of four-phased current for 3 N.m at 500 rpm

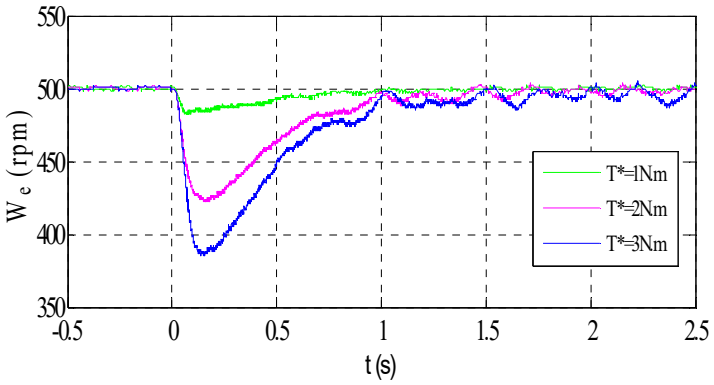

Fig. 15 Experimental speed responses; disturbance rejection at 500 rpm

VI. Conclusion

In this paper, a H-infinity current controller has been designed for an 8/6 SRM. To cope with the nonlinear character of the SRM, a stage of adaptation has been added to complete the control loop. This adaptation compensates the variation of the phase inductance of the SRM, which strongly depends on the rotor position and the phase current. The validation of this control was performed first by means of simulations. The robustness and performances of the control were evaluated and compared with those of a PI controller by using analysis in frequency domain. Simulations results show that the H_∞ controller ensures better stability of the dynamic system under varying the phase inductance. Finally, experimental tests were carried out by using an experimental test bench. The obtained results demonstrate that the designed controller gives good performances in tracking and in rejection disturbances. In future work, it would be interesting to use μ-analysis in order to analyze with a better accuracy the uncertainties in parameters and their effect on the frequency evolution.

References

[1] Piyush C. Desai; Mahesh Krishnamurthy; Nigel Schofield; Ali Emadi: Switched Reluctance Machines with higher rotor poles than stator poles for improved output torque characteristics, Industrial Electronics, 2009. IECON '09. 35th Annual Conference of IEEE , pp.1338-1343, Nov 2009, Portugal.

[2] M. W. Arab; E. Godoy; I. Bahri; M. Hilairet; P. García Estébanez; S. A. Randi : Current Controller for Switched Reluctance Motors Using Pole Placement Approach, Electric Machines & Drives Conference (IEMDC), 2013 IEEE International, pp 1119 – 1125, May 2013, Chicago.

[3] H. Yang, S.K. Panda, and Y.C. Liang: Experimental investigation of feedback linearization controller for switched reluctance motor, IEEE 27th Annual Power Electronics Specialists Conference, PESC '96, vol.2, pp.1804–1810, Juin 1996, Italy.

[4] Espinosa-Perez, P. Maya-Ortiz, M. Velasco-Villa, and H. Sira-Ramirez.: Passivity-based control of switched reluctance motors with nonlinear magnetic circuits, Proceedings of the 41st IEEE Conference on Decision and Control, vol.1, pp.468–473, May 2004.

[5] Yuefeng Yang, Yihuang Zhang: Sliding mode-PI control of switched reluctance motor drives for EV, International Conference on Electrical Machines and Systems, vol. 1, no. 1, pp.603-607, Sept 2015

[6] Hannoun, M. Hilairet, and C. Marchand, "High performance current control of a switched reluctance machine based on a gain-sheduling PI controller," Control Engineering Practice, vol.19, no.11, pp.1377-1386, Nov.2011.

[7] M. R. Benhadria, K. Kendouci, and B. Mazari: Torque ripple minimization of switched reluctance motor using hysteresis current control, IEEE International Symposium on Industrial Electronics, vol.3 pp.2158–2162, July 2006, Montréal

[8] K. Dong-Hee, J.Hae-Gwang, L.Kyo-Beum: Torque Ripple Minimization of Switched Reluctance Motors Based on Fuzzy Logic and Sliding Mode Control, Industrial Electronics (ISIE), pp. 1 – 6, 2013.

[9] N. Ouddah, M. Boukhnifer, A. Chaibet, E. Monmasson and E. Berthelot: Experimental Robust H∞ Controller Design of Switched Reluctance Motor for Electrical Vehicle Application, 2014 IEEE Conference on Control Applications (CCA) Part of 2014 IEEE Multi-conference on Systems and Control, pp. 1570 – 1575, October 8-10, 2014. Antibes, France.

[10] Nadir Ouddah, Moussa Boukhnifer, Ahmed Chaibet and Eric Monmasson: Robust Controller Designs of Switched Reluctance Motor for Electrical Vehicle, 2014 22ndMediterranean Conference on Control and Automation (MED) University of Palermo, pp. 212 – 217, June 16-19, 2014. Palermo, Italy.